

MIT Open Access Articles

*Dynamic Fluid-Like Graphene with
Ultralow Frictional Molecular Bearing*

The MIT Faculty has made this article openly available. **Please share** how this access benefits you. Your story matters.

Citation: Intak, Jeon et al. "Dynamic Fluid-Like Graphene with Ultralow Frictional Molecular Bearing." *Advanced Materials* 31, 43 (September 2019): 1903195 © 2019 Wiley

As Published: <http://dx.doi.org/10.1002/adma.201903195>

Publisher: Wiley

Persistent URL: <https://hdl.handle.net/1721.1/128131>

Version: Author's final manuscript: final author's manuscript post peer review, without publisher's formatting or copy editing

Terms of use: Creative Commons Attribution-Noncommercial-Share Alike



DOI: 10.1002/((please add manuscript number))

Article type: Communication

Dynamic Fluid-like Graphene with Ultra-Low Frictional Molecular Bearing

Intak Jeon^{1,2†}, Geehoon Park^{3†}, Pan Wang^{1,2}, Ju Li^{4,5}, Ian W. Hunter^{3*}, and Timothy M. Swager^{1,2*}*

Dr. I. Jeon, Dr. P. Wang, Prof. T. M. Swager
Department of Chemistry
Institute for Soldier Nanotechnologies
Massachusetts Institute of Technology
Cambridge, MA 02139, USA
E-mail: tswager@mit.edu

G. Park, Prof. I. W. Hunter
Department of Mechanical Engineering
Massachusetts Institute of Technology
Cambridge, MA 02139, USA
E-mail: ihunter@mit.edu

Prof. J. Li
Department of Nuclear Science and Engineering
Department of Materials Science and Engineering
Massachusetts Institute of Technology
Cambridge, MA 02139, USA
E-mail: liju@mit.edu

†These authors contributed equally to this work.

Keywords: fluid-like graphene, ultra-low friction, molecular bearing, coefficient of friction of 0.01, triptycene

Abstract: Fluid-like sliding graphenes but with solid-like out-of-plane compressive rigidity offer unique opportunities for achieving unusual physical and chemical properties for next generation interfacial technologies. Of particular interest in the present study are graphenes with specific chemical functionalization that can predictably promote adhesion and wetting to substrate and ultra-low frictional sliding structures. We experimentally demonstrate lubricity between stainless steel (SS) and diamond-like-carbon (DLC) with densely functionalized graphenes displaying dynamic intersheet bonds that mechanically transform into stable tribolayers. The macroscopic lubricity evolves through the formation of a thin film of an interconnected graphene matrix that provides a coefficient of friction (COF) of 0.01.

1 Mechanical sliding generates complex folded graphene structures wherein equilibrated
2 covalent chemical linkages impart rigidity and stability to the films examined in macroscopic
3 friction tests. This new approach to frictional reduction has broad implications for
4 manufacturing, transportation, and aerospace.
5
6
7
8
9

10 11 **Article**

12
13
14
15 The development of advanced superlubricant materials, defined by a coefficient of
16 friction (COF) near or lower than 0.01, is essential for the sustainability and achieving higher
17 performance from mechanical devices.^[1-3] Although pristine graphene has a desirable
18 incommensurability in its lattice plane relative to other materials and can suppress mechanical
19 wear,^[4-9] the creation of incommensurate stable contacts at macroscale interfaces still poses
20 fundamental challenges. In particular, superior lubricant materials will have both the
21 properties of a liquid and a solid.^[10-14] At one extreme, a thin layer of a liquid (water) can
22 behave as a lubricant, and hydroplaning behavior reduces frictional contact between tires and
23 a road.^[15] Inspired by hydroplaning and graphite, we have designed a fluid-like reconfigurable
24 graphene matrix that shows quasi-hydrodynamic and ultra-low frictional behavior. We
25 hypothesized that the graphene matrix with chemically dynamic (reversible) connections
26 can transform into molecular bearings that simultaneously have a large resistance to further
27 compression and a stable top-surface with sustained lubricity with ultra-low friction.
28
29
30
31
32
33
34
35
36
37
38
39
40
41
42
43
44
45
46
47

48 To create a scalable ultra-low frictional material, we designed a coating wherein basal
49 plane functionalized graphenes, produced by electrochemical activation, are covalently
50 attached to structurally rigid triptycene molecular cores. Specifically the interconnected
51 graphene matrix is produced by the reactive formation of Meisenheimer complexes between
52 graphene functionalized with 3,5-dinitrophenyl groups and triaminotriptycene (**Triamino-**
53 **T**).^[16, 17] **Triamino-T** was designed as a highly stable rigid 3D interlocking group that
54
55
56
57
58
59
60
61
62
63
64
65

1 reversibly covalently links reactive functionalized graphenes into an interconnected matrix
2 that is dynamically configured by physical sliding motions. The COF of the resultant
3 triaminotriptycene functionalized graphene (**FG-T**) reaches the ultra-low regime (0.01),
4 whereas graphene functionalized with 3,5-dinitrophenyl groups, but lacking **Triamino-T**
5 modification, shows a higher and erratic friction as a result of chemical interactions with the
6 interacting surfaces. The 3,5-dinitrophenyl functionalized graphene is reacted with **Triamino-**
7 **T** to give a material (**FG-T+**) that evolves into stable self-leveling tribo-layers during sliding.
8 The structural re-arrangement of the graphene matrix provides a mechanism to achieve robust
9 superlubricity at both the micro- and macro-scale.
10
11
12
13
14
15
16
17
18
19
20
21

22 The **FG-T+** composition (**Figure 1a** and **Figure S1**) undergoes reversible
23 Meisenheimer complexation reactions that provide a reconfigurable interlocking component.
24 Here the NH₂ groups of the **Triamino-T** can be bonded to up to three different 3,5-
25 dinitrophenyl groups, and the stoichiometry of **FG-T+** ensures residual reactive primary
26 amines (**Figure S2**). The **FG-T+** film structure equilibrates through transient chemical
27 configurations when mechanical shearing (sliding motion) is applied to the material. The
28 reversible reconfiguration of the films under sliding against a DLC-coated ball further enables
29 self-leveling (recoating) of damaged regions (**Figure S3**), which demonstrate strong adhesion
30 and "complete wetting" between **FG-T+** and steel substrate. The final matrix contains a
31 highly crosslinked **FG-T** network with 3D rigid triptycene interlocking units between
32 graphene sheets bond in Meisenheimer complexes (**Figure 1a**).^[18] We postulate that the **FG-**
33 **T+** film is segmented into viscous films on the top-surfaces, and a core connection to the
34 substrate through the elastic graphene matrix. These layers help to induce viscous flow on
35 top-surface and to guard against wear, thereby producing quasi-hydrodynamic behavior with
36 reduced friction.^[19]
37
38
39
40
41
42
43
44
45
46
47
48
49
50
51
52
53
54
55
56
57
58
59
60
61
62
63
64
65

1 The solid 3,5-dinitrophenyl functionalized graphene (**FG**) film shows transient shear
2 thinning behavior (**Figure 1b**). Conversely, dynamic linkages of **FG-T+** lead to Newtonian
3 fluid-like behavior, perhaps promoted by the equilibrating Meisenheimer complexation and
4 the associated changes in graphene structure (**Figure 1b**). The addition of excess **Triamino-T**
5 lowers the viscosity from the beginning shear rate of 5.0 s^{-1} , and this behavior for the **FG-T+**
6 films is consistent with energy dissipation as a result of dynamic rearrangement of the
7 Meisenheimer complexes (**Figure 1b**).^[20, 21]

8
9
10
11
12
13
14
15
16
17 To further probe viscoelastic properties of these reversible and reconfigurable
18 complexes we have determined the storage modulus (G') and loss modulus (G'') at different
19 frequencies of oscillating strain. **FG** and **FG-T** show a predominant elastic response over the
20 entire frequency range ($G' \gg G''$), whereas the viscoelastic behavior of **FG-T+** shows
21 continuous changes over the frequency spectrum investigated (**Figure 1c**). In case of **FG**, we
22 note that the decrease in the loss modulus at 7 rad s^{-1} is consistent with chemical degradation,
23 wherein continuous shearing induces mechanochemical reactions on graphene. Subsequent
24 mechanochemical damage or physical removal of material, results in further change the loss
25 modulus contribution during shearing (*vide infra*). The gradual increases in the viscoelastic
26 response of the **FG-T+** film is consistent with our proposed chemical/structural evolution that
27 occurs without chemical degradation. In total the rheological results are self-consistent with
28 reversible Meisenheimer complex formation between the triptycenes and graphene to give a
29 fluid-like matrix for reducing frictional behavior. These mechanical dynamics offer insights
30 into the kinetics of the reconfigurable bonding in functional graphenes.
31
32
33
34
35
36
37
38
39
40
41
42
43
44
45
46
47
48
49
50
51
52
53
54
55
56
57
58
59
60
61
62
63
64
65

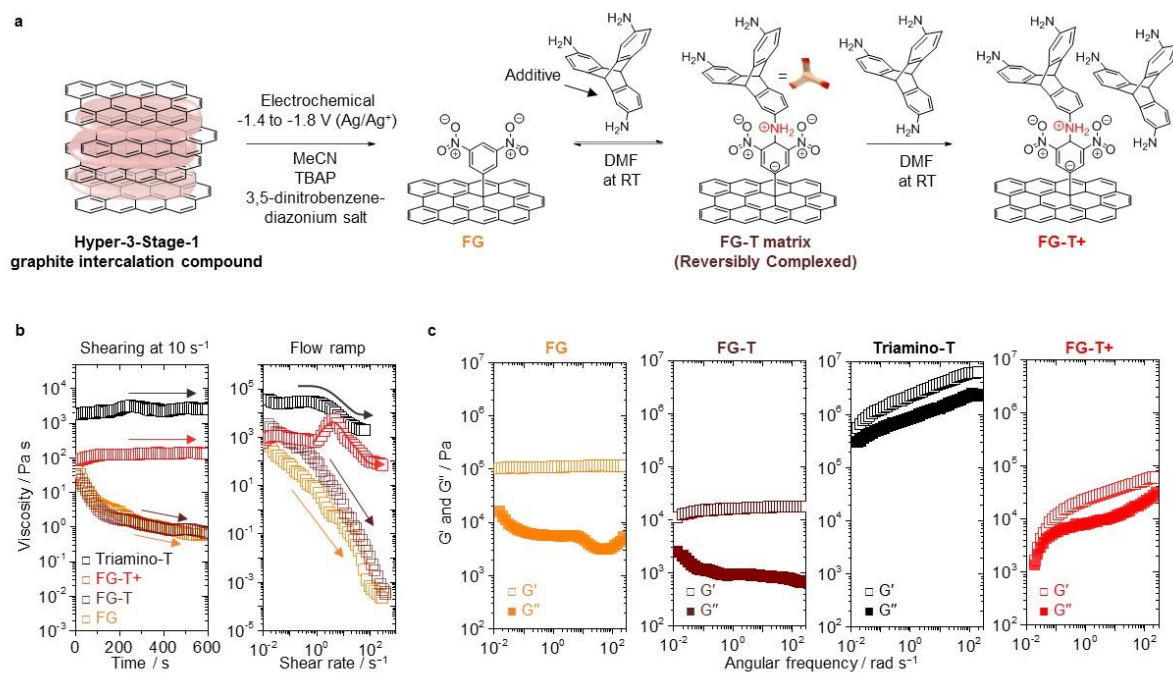


Figure 1. Fluid-like reconfigurable graphene. (a) Synthesis and chemical structures of FG, FG-T, and FG-T+. FG-T is synthesized via Meisenheimer complexes reaction with Triamino-T. FG-T+ contains the additional concentration of Triamino-T (additive) such that there are free amine groups that are not covalently linked to the graphene. MeCN: acetonitrile, TBAP: tetrabutylammonium perchlorate and DMF: dimethylformamide. (b) Time-dependent viscoelastic behaviors of FG, FG-T, Triamino-T, and FG-T+: Shearing at the shear rate of 10 s⁻¹ for 10 mins. The FG and FG-T continuously decrease in viscosity with increased shear rate. The viscosity–shear strain rate curves: Triamino-T (black arrow) show shear thickening behaviors. After reconfiguration (red arrow), the FG-T+ stabilizes and approaches a Newtonian behavior because the graphene matrix with triptycenes can rearrange to accommodate stress. (c) Linear viscoelastic behavior: Change in storage (G') and loss (G'') moduli versus angular frequency (ω) with the strain of $\gamma = 0.5\%$ for FG, FG-T, FG-T+ and Triamino-T, demonstrating the reconfigurable viscoelastic mechanism of the FG-T+ matrix.

1 Friction tests were conducted by coating stainless steel (SS) with the different
2 graphenes and sliding a diamond like carbon (DLC) coated SS ball, using a custom-built
3 linear macro-tribometer (**Figure 2a and Figure S4**). Initially, the COF of unfunctionalized
4 exfoliated low defect graphene (**UEG**) is ~ 0.022 (**Figure 2b**), a value comparable to the
5 previously reported graphenes and graphene oxides (GOs), thereby confirming the system's
6 performance (**Figure S5**).^[22-24] The **UEG** is produced from a dimethylformamide dispersion
7 of a Hyper-3-Stage-1 graphite intercalation compound (GIC),^[16] and although it forms a low
8 frictional tribo-layer, the stability of the tribo-layer on the SS substrate was not satisfactory, as
9 it easily peels off or ball up on the substrate, showing poor adhesion and incomplete wetting.
10 To create a stable layer, the coating materials need to remain strongly associated with the
11 surface during mechanical movement (**Figure S6**). In case of **UEG** coatings on the SS
12 substrate, large spikes in the COF ~ 0.1 appear by about 1500 cycles, indicating removal of
13 graphene tribo-layer as a result of weak adhesion to the substrate (**Figure 2b**). These spikes
14 appear at random intervals, are frequency and magnitude dependent, and are a signature of
15 insufficient adhesion to the SS surface (**Figure S7**). The high contact pressures and linear
16 motion give rise to a natural gradual loss of graphene coverage from metallic substrates in
17 macroscopic friction tests. As a result, graphene tribo-layers can undergo detrimental
18 transformations in very short periods. These adhesion challenges are the reason that typical
19 multilayer graphene systems, which are nominally expected to have the low frictional
20 properties, fail to provide stable superlubricity.^[7]

21 **FGs** in general have enhanced interactions with most substrate materials and hence
22 have utility for increasing the stability of a tribofilm (**Figure 2b**). However, the high COF
23 observed for the **FG** used in this study appears to produce adhesive interactions between
24 contacting materials, but without special additives, this material degrades and does not
25 produce stable tribofilms in the friction tests. These results are consistent with previous

1 atomic force microscopy (AFM) friction measurements on fluorinated graphene,^[25, 26]
2 wherein functionalized graphene monolayers exhibited higher friction forces relative to
3 pristine graphene. In short, the friction originates from basal plane functional groups that
4 increase van der Waals interactions. To overcome these seemingly intrinsic limitations
5 associated with functionalized graphene, we targeted the generation of dynamic
6 nanostructures to realize a stable ultra-low frictional state.
7
8
9
10
11
12
13
14

15 The **FG-T** matrix relaxes under applied stress through reversible chemical bonding
16 events with **Triamino-T**. We observed the further reduction in COFs with **FG-T+**, which
17 produces an ultra-low frictional state (**Figure 2b and c**) comparable to **UEG-nanodiamond**
18 combinations (**Figure S8**).^[22] We attributed this result to the reconfiguration of the stable
19 graphene matrix, wherein the molecular crosslinker connects graphene surfaces and stabilizes
20 bilayers and/or folded structures to create dynamic “molecular-bearings” with mechanical
21 stiffness and stability (**Figure 2d and Figure S9**). This process gives a dense stable tribo-
22 layer with liquid-like properties that allows for self-leveling of the lubricant layer, to
23 counteract the continuous mechanical removal caused by the sliding and pressure gradient. In
24 contrast to **FG-T/FG-T+**, the mixture of **UEG** and **Triamino-T** (**UEG-T**) exhibits unstable
25 sliding behavior due to the lack of the chemical function for stabilizing bearing molecules
26 (**Figure 2b and d**). The friction coefficient of **FG-T+** stabilizes at 0.011 at 16 mm s⁻¹ and
27 drops to 0.01 at 26 mm s⁻¹ (**Figure 2e**). The **FG-T+** also shows low frictional behavior (COF
28 < 0.015) at loads varying from 3 N to 1.1 N (**Figure 2f**). After long-term cycles, we observed
29 the lower wear rate of DLC-coated SS ball against a **FG-T+** ($0.94 \times 10^{-9} \text{ mm}^3 \text{ N}^{-1} \text{ m}^{-1}$) on SS
30 as compared to uncoated SS ($9.94 \times 10^{-9} \text{ mm}^3 \text{ N}^{-1} \text{ m}^{-1}$) (**Figure S10**). **FG-T+** also
31 outperformed an uncoated SS in ambient air and initially showed reduced friction for a SS/SS
32 pair (**Figure S11**).
33
34
35
36
37
38
39
40
41
42
43
44
45
46
47
48
49
50
51
52
53
54
55
56
57
58
59
60
61
62
63
64
65

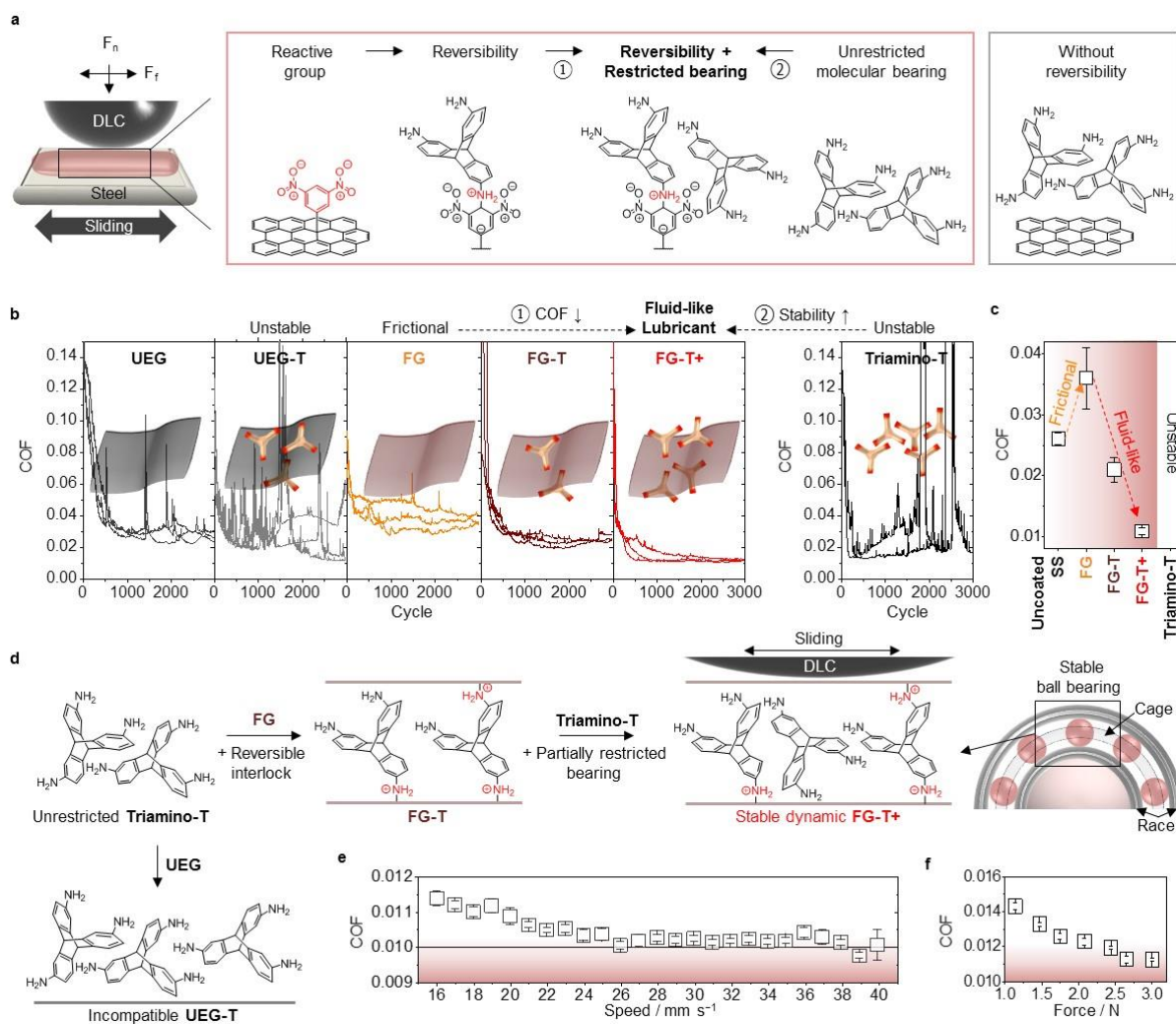


Figure 2. Illustration of COF and results for graphene films. (a) Schematic illustration showing the geometry of a linear tribometer equipped with a DLC-coated stainless steel ball. The friction tests were performed with graphenes and/or **Triamino-T** to demonstrate the synergetic coupling effect of reversible Meisenheimer complexes and molecular bearings. (b) The COF for a DLC ball sliding at 16 mm s⁻¹ and a contact pressure of 0.3 ~ 0.4 GPa, against **UEG** (COF ~ 0.022 ± 0.003), **UEG-T** (COF: unstable), **FG** (COF ~ 0.036 ± 0.005), **FG-T** (COF ~ 0.021 ± 0.002), **FG-T+** (COF ~ 0.011 ± 0.001) and **Triamino-T** (COF: unstable) films on a SS substrate in N₂ environment (relative humidity: ~ 3 %). Friction experiments were repeated three or more times for each sample (one cycle = two linear-sliding motions). (c) The average COF of the uncoated SS, **FG**, **FG-T**, **FG-T+** and **Triamino-T** films. (d) The proposed dynamic model of reversible Meisenheimer complexation of graphene with **Triamino-Ts** to create reconfigurable networks “bearing” behavior. First, unrestricted **Triamino-T** shows unstable sliding motion with temporary low COF in our system. Second, the incompatibility of **UEG-T** restricts the formation of a stable matrix during sliding. Third, the molecular bearing motion of partially restricted **Triamino-T** is effectively stabilized in a dynamic **FG-T/FG-T+** matrix, maintaining low COF. (e) The **FG-T+** friction with increasing sliding speed tests from 16 mm s⁻¹ to 40 mm s⁻¹ with ≈ 0.01 above a 26 mm s⁻¹ sliding speed in the quasi-hydrodynamic lubrication regime. (f) Load dependency of the COF of **FG-T+**.

1
2
3
4
5
6
7
8
9
10
11
12
13
14
15
16
17
18
19
20
21
22
23
24
25
26
27
28
29
30
31
32
33
34
35
36
37
38
39
40
41
42
43
44
45
46
47
48
49
50
51
52
53
54
55
56
57
58
59
60
61
62
63
64
65

To gain insight on the tribochemical reactions and how **FG-T** and **FG-T+** promote stable ultra-low frictional states, we have conducted Raman and XPS analyses of the as deposited materials and the mechanically produced tribo-layers (**Figure 3** and **Figure S12**).^[16, 27, 28] In general, graphenes slip by each other and then evolve into graphene tribo-layers with the reduced COF against the DLC-coated ball.^[7, 29] The final state of graphene on a SS substrate after sliding can produce changes in the Raman 2D and D-bands, which are quantified by the D-band to the G-band ratio, I_D/I_G . An increasing I_D/I_G indicates the introduction of defects in the graphene layers (**Figure 3a**), and this is readily apparent for **UEG**. In addition, the G-band (1591 cm^{-1}) for the lubricated graphene shifts after sliding, compared with that of pristine graphene (1580 cm^{-1}), which also indicates changes in chemical or physical state.^[16, 30] This is expected as the G-band is sensitive to damage within the graphene sheets. Additionally, XPS analysis reveals increases in the relative ratios of sp^3 C–C ($\sim 285.5\text{ eV}$) to sp^2 C–C peaks ($\sim 284.5\text{ eV}$), which is also an indication of mechanically induced chemistry (**Figure 3a**).

FG initially has a high density of pendant groups (Raman I_D/I_G ratio ~ 0.93 in **Figure 3b**) with a stronger interaction with the DLC surface and a higher frictional resistance toward sliding. The nitrogen-containing functional groups are removed with sliding (**Figure 3b**) and the XPS N 1s signals associated with functional groups on the surface of graphene are not detectable after sliding. However, the XPS signals associated with sp^3 carbons ($\sim 285.5\text{ eV}$) and the Raman I_D/I_G remains high (**Figure 3b** and **Figure S9**). The fate of removed nitrogen containing functional groups and the nature of the sp^3 Cs are not known, however mechanochemical reactions are expected under the applied load.^[26, 31-33]

The addition of the triptycene stabilizes the 3,5-dinitrophenyl groups on the graphene and in contrast to **FG** the XPS N 1s signals associated with the 3,5-dinitrophenyl functional groups of **FG-T** and **FG-T+** are retained after sliding (**Figure 3c** and **d**). Although it is a

challenge to experimentally probe the precise physical and chemical interior states of the graphene matrix, it would appear that **FG-T+** is stabilized by the dynamic covalent chemically interlocking reactions within the material (**Figure S9**).^[34]

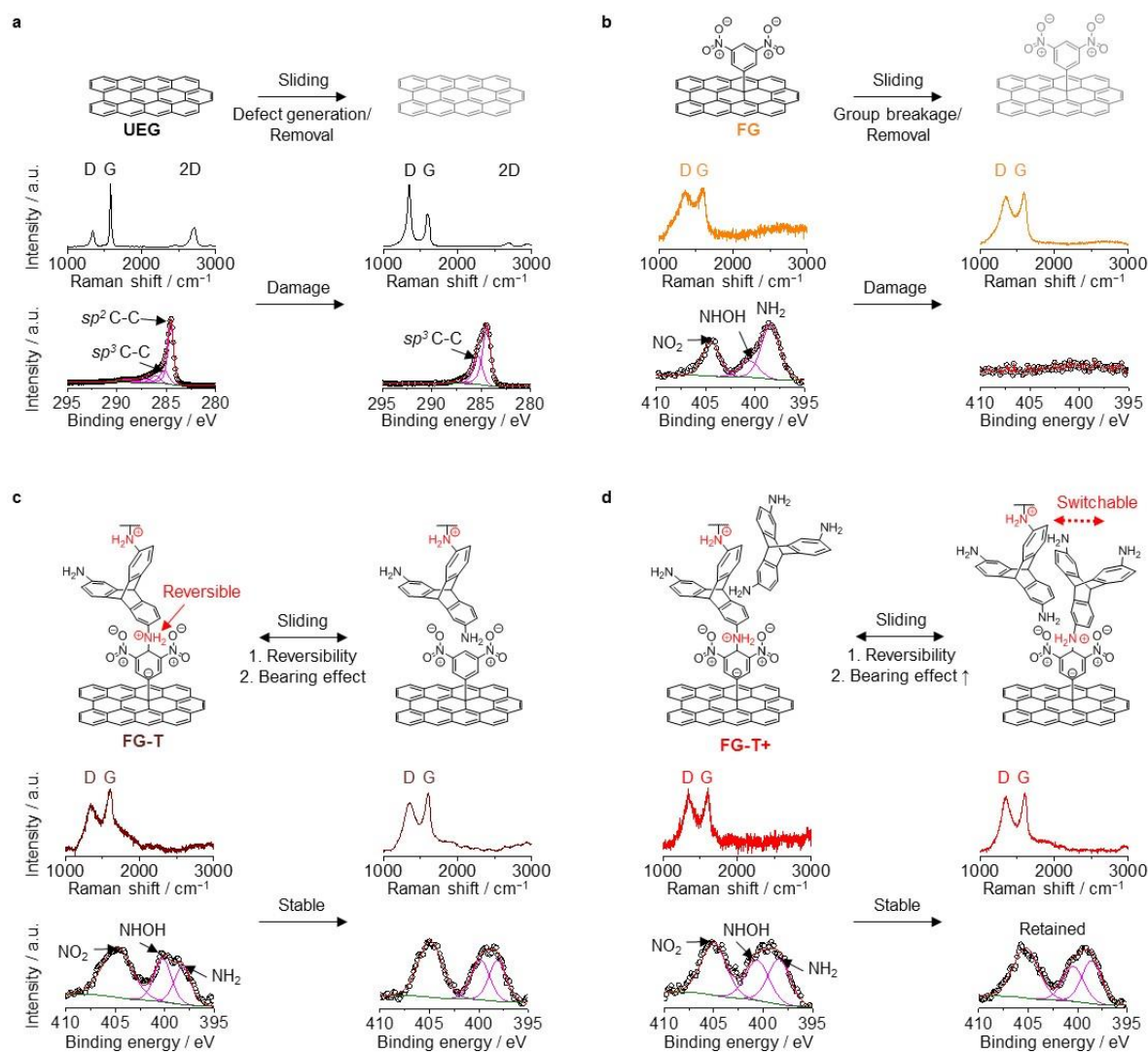


Figure 3. Mechanically induced chemical transitions of graphene films. Raman and XPS spectra of (a) UEG, (b) FG, (c) FG-T, and (d) FG-T+ before and after sliding cycles that detail characteristic changes. The tribo-layer of fluid-like FG-T+ is stabilized during sliding motion due to the reversibility of FG-T+ into contacting edges and self-leveling. The solid-like FG and UEG undergo tribo-chemically damage as evidenced by changes in their spectral properties.

1
2
3
4
5
6
7
8
9
10
11
12
13
14
15
16
17
18
19
20
21
22
23
24
25
26
27
28
29
30
31
32
33
34
35
36
37
38
39
40
41
42
43
44
45
46
47
48
49
50
51
52
53
54
55
56
57
58
59
60
61
62
63
64
65

Tribo-layers are produced after sliding tests as shown in **Figure 4**. Scanning electron microscope (SEM) images (**Figure 4a and Figure S6**) reveal that with frictional testing the graphene is partially removed and reconfigured. The formation of a stable surface-bonded tribo-layer at a contacting surface reduces wear by minimizing contact of material pairs.^[35] Our lubricant with its quasi-hydrodynamic nature, is initially in a form that can be characterized as crumpled graphene nanoballs. The mechanical sliding under load then leads to a coalescence of particles to produce continuous solid lubricant film that strongly adheres to and completely wets the substrate. The very rigid framework within these films results from the interlinking of graphenes by Meisenheimer complexation.

To observe the structural progression of our graphene lubricant, we performed microstructure and surface analyses of tribo-layers after sliding using transmission electron microscopy (TEM) and atomic force microscopy (AFM) (**Figure 4 and Figure S13**).^[36-38] As shown in **Figure 4b**, that graphenes initially appear as a continuous interconnected material (**Figure 4b**). During sliding at a stress of 0.4 GPa, the matrix undergoes compression and structurally evolves from a spherical configuration to compressed interconnected layers that have a spacing of 11.6 Å, which is consistent with the interlayer organic linkages (**Figure 4c**). The tribo-layer of **FG-T+** produced by the sliding, is reasonably flat with ± 5 nm surface features (**Figure 4d and Figure S14**), which is also consistent with a compressed layered structure. This planar tribo-layer allows DLC to slide and only encounter relatively small energetic barriers. The high out-of-plane rigidity of the **FG-T+** tribo-layer is also critical and compares favorably to the bare SS (grade 316). Nanoindentation reveals a hardness with ~ 5.3 GPa for the SS 316 substrate and ~ 7.3 GPa for the tribo-layer of **FG-T+** (**Figure 4e**). The higher value of hardness is also consistent with a strongly textured **FG-T+** tribo-layer.

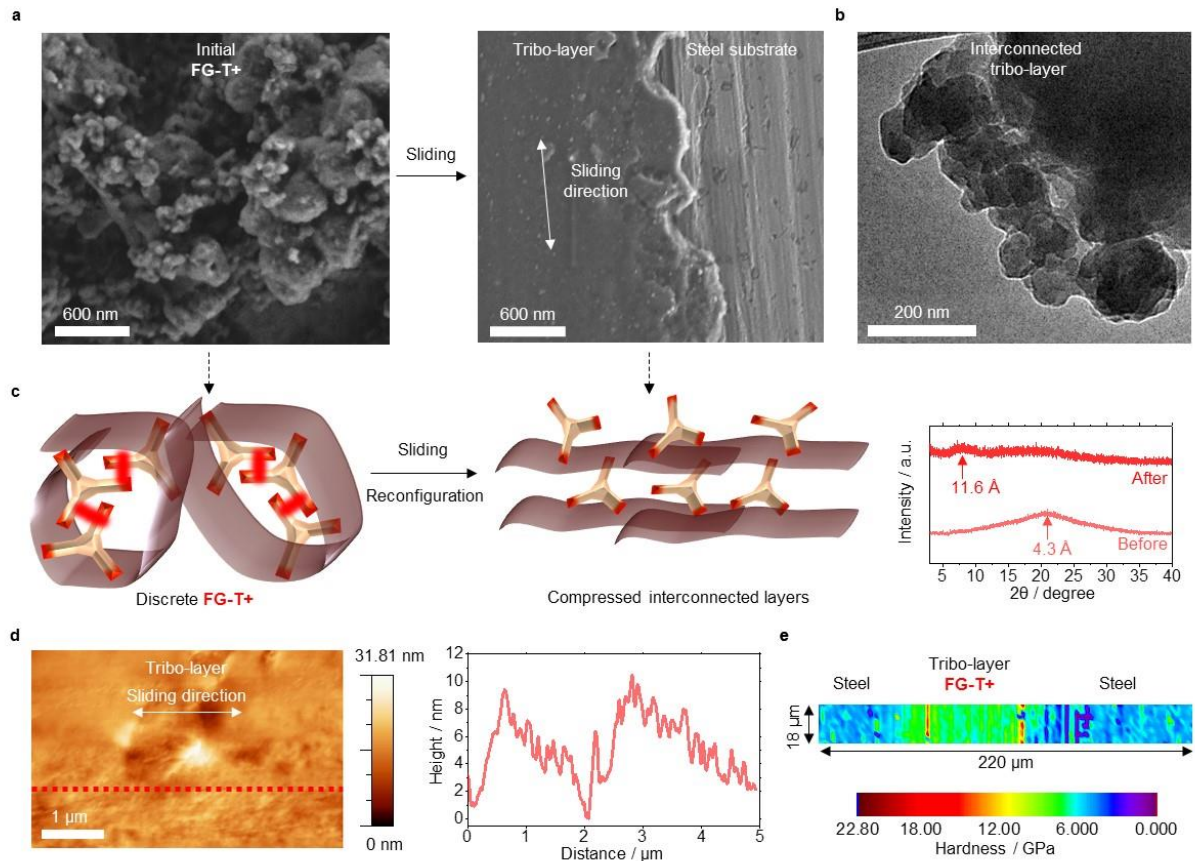


Figure 4. The representative microstructure of FG-T+ matrix after sliding. (a) SEM image of *as-prepared* FG-T+ before sliding and the tribo-layer after sliding. (b) TEM image of the tribo-layer of FG-T+. The formation of continuous FG-T+ matrix is observed. (c) Left: *as-prepared* FG-T+ matrix is proposed to be in a compacted folded structure. Right: After its sliding test FG-T+ is expected to have more of a compressed bi/multi-layer structure, which is supported X-ray diffraction data. (d) Tapping-mode AFM topography image of the top-surface of the tribo-layer. The AFM height profile measured along the red dashed line. The tribo-layer of FG-T+ has a flattened surface. (e) A nanoindentation map displays the hardness of the representative FG-T+ tribo-layer, using a Berkovich diamond indenter.

In summary, we have demonstrated that FG-T+ forms a fluid-like graphene matrix that produce stable tribo-layers and a low frictional force against the DLC (COF ~ 0.01). The dynamic reactivity and flexibility of functional graphene and the rigid frame of triptycene combine to produce adherent and shearing structures under compressive sliding deformation.

This approach to an ultra-low frictional state is potentially generalizable and is an important step to understanding how to control friction at the macroscale.

Supporting Information

Supporting Information is available from the Wiley Online Library or from the author.

Acknowledgements

T. Swager, J. Li, and I. Hunter directed the project. I. Jeon synthesized graphene materials and G. Park constructed the friction measurement apparatus. I. Jeon and G. Park carried out experiments and the data analysis. P. Wang synthesized triamimotriptycene. All the authors discussed the results and contributed to the writing of the manuscript. I. Jeon and G. Park contributed equally to this work. This work was supported by the US Army Research Office through the use of facilities at the Institute for Soldier Nanotechnologies under Contract Number W911NF-13-D-0001 and National Science Foundation, DMR-1809740. We appreciate Maggie He for synthesizing the 3,5-dinitrobenzenediazonium salt.

Received: ((will be filled in by the editorial staff))

Revised: ((will be filled in by the editorial staff))

Published online: ((will be filled in by the editorial staff))

References

- [1] S. C. Tung, M. L. McMillan, *Tribol. Int.* **2004**, *37*, 517.
- [2] K. Holmberg, P. Andersson, A. Erdemir, *Tribol. Int.* **2012**, *47*, 221.
- [3] S. F. Tie, C. W. Tan, *Renew. Sust. Energ. Rev.* **2013**, *20*, 82.
- [4] C. Lee, Q. Y. Li, W. Kalb, X. Z. Liu, H. Berger, R. W. Carpick, J. Hone, *Science* **2010**, *328*, 76.
- [5] S. Kawai, A. Benassi, E. Gnecco, H. Sode, R. Pawlak, X. L. Feng, K. Mullen, D. Passerone, C. A. Pignedoli, P. Ruffieux, R. Fasel, E. Meyer, *Science* **2016**, *351*, 957.
- [6] M. Dienwiebel, N. Pradeep, G. S. Verhoeven, H. W. Zandbergen, J. W. M. Frenken, *Surf. Sci.* **2005**, *576*, 197.
- [7] S. Z. Li, Q. Y. Li, R. W. Carpick, P. Gumbsch, X. Z. Liu, X. D. Ding, J. Sun, J. Li, *Nature* **2016**, *539*, 541.
- [8] M. S. Won, O. V. Penkov, D. E. Kim, *Carbon* **2013**, *54*, 472.
- [9] Y. Z. Qi, J. Liu, J. Zhang, Y. L. Dong, Q. Y. Li, *ACS Appl. Mater. Inter.* **2017**, *9*, 1099.
- [10] I. R. Peters, S. Majumdar, H. M. Jaeger, *Nature* **2016**, *532*, 214.
- [11] V. Trappe, V. Prasad, L. Cipelletti, P. N. Segre, D. A. Weitz, *Nature* **2001**, *411*, 772.
- [12] X. Cheng, J. H. McCoy, J. N. Israelachvili, I. Cohen, *Science* **2011**, *333*, 1276.
- [13] J. M. Brader, *J Phys-Condens Mat* **2010**, *22*, 363101.
- [14] J. Vermant, M. J. Solomon, *J Phys-Condens Mat* **2005**, *17*, R187.
- [15] D. Mohrig, K. X. Whipple, M. Hondzo, C. Ellis, G. Parker, *Geol Soc Am Bull* **1998**, *110*, 387.
- [16] I. Jeon, B. Yoon, M. He, T. M. Swager, *Adv. Mater.* **2018**, *30*, 1704538.
- [17] T. M. Swager, *Acc. Chem. Res.* **2008**, *41*, 1181.
- [18] F. Terrier, *Chem. Rev.* **1982**, *82*, 77.
- [19] H. Heshmat, *Lubr Eng* **1992**, *48*, 373.
- [20] F. Del Giudice, A. Q. Shen, *Curr Opin Chem Eng* **2017**, *16*, 23.
- [21] S. B. Kharchenko, J. F. Douglas, J. Obrzut, E. A. Grulke, K. B. Migler, *Nat. Mater.* **2004**, *3*, 564.
- [22] D. Berman, S. A. Deshmukh, S. K. R. S. Sankaranarayanan, A. Erdemir, A. V. Sumant, *Science* **2015**, *348*, 1118.

- 1 [23] K. S. Kim, H. J. Lee, C. Lee, S. K. Lee, H. Jang, J. H. Ahn, J. H. Kim, H. J. Lee, *ACS*
2 *Nano* **2011**, *5*, 5107.
- 3 [24] D. Berman, A. Erdemir, A. V. Sumant, *Mater. Today* **2014**, *17*, 31.
- 4 [25] Q. Y. Li, X. Z. Liu, S. P. Kim, V. B. Shenoy, P. E. Sheehan, J. T. Robinson, R. W.
5 Carpick, *Nano Lett.* **2014**, *14*, 5212.
- 6 [26] S. Kwon, J. H. Ko, K. J. Jeon, Y. H. Kim, J. Y. Park, *Nano Lett.* **2012**, *12*, 6043.
- 7 [27] M. J. Webb, P. Palmgren, P. Pal, O. Karis, H. Grennberg, *Carbon* **2011**, *49*, 3242.
- 8 [28] E. Bekyarova, M. E. Itkis, P. Ramesh, C. Berger, M. Sprinkle, W. A. de Heer, R. C.
9 Haddon, *J. Am. Chem. Soc.* **2009**, *131*, 1336.
- 10 [29] X. F. Feng, S. Kwon, J. Y. Park, M. Salmeron, *ACS Nano* **2013**, *7*, 1718.
- 11 [30] O. Frank, G. Tsoukleri, J. Parthenios, K. Papagelis, I. Riaz, R. Jalil, K. S. Novoselov,
12 C. Galiotis, *ACS Nano* **2010**, *4*, 3131.
- 13 [31] S. L. James, C. J. Adams, C. Bolm, D. Braga, P. Collier, T. Friscic, F. Grepioni, K. D.
14 M. Harris, G. Hyett, W. Jones, A. Krebs, J. Mack, L. Maini, A. G. Orpen, I. P. Parkin, W. C.
15 Shearouse, J. W. Steed, D. C. Waddell, *Chem. Soc. Rev.* **2012**, *41*, 413.
- 16 [32] J. R. Felts, A. J. Oyer, S. C. Hernandez, K. E. Whitener, J. T. Robinson, S. G. Walton,
17 P. E. Sheehan, *Nat. Commun.* **2015**, *6*, 6467.
- 18 [33] L. F. Wang, T. B. Ma, Y. Z. Hu, H. Wang, *Phys. Rev. B* **2012**, *86*, 125436.
- 19 [34] A. D. Cambou, N. Menon, *Proc. Natl. Acad. Sci. USA* **2011**, *108*, 14741.
- 20 [35] N. N. Gosvami, J. A. Bares, F. Mangolini, A. R. Konicek, D. G. Yablon, R. W.
21 Carpick, *Science* **2015**, *348*, 102.
- 22 [36] A. C. Ferrari, *Solid State Commun.* **2007**, *143*, 47.
- 23 [37] Q. Z. Wu, Y. P. Wu, Y. F. Hao, J. X. Geng, M. Charlton, S. S. Chen, Y. J. Ren, H. X.
24 Ji, H. F. Li, D. W. Boukhvalov, R. D. Piner, C. W. Bielawski, R. S. Ruoff, *Chem. Commun.*
25 **2013**, *49*, 677.
- 26 [38] A. C. Ferrari, J. C. Meyer, V. Scardaci, C. Casiraghi, M. Lazzeri, F. Mauri, S.
27 Piscanec, D. Jiang, K. S. Novoselov, S. Roth, A. K. Geim, *Phys. Rev. Lett.* **2006**, *97*, 187401.
- 28
29
30
31
32
33
34
35
36
37
38
39
40
41
42
43
44
45
46
47
48
49
50
51
52
53
54
55
56
57
58
59
60
61
62
63
64
65

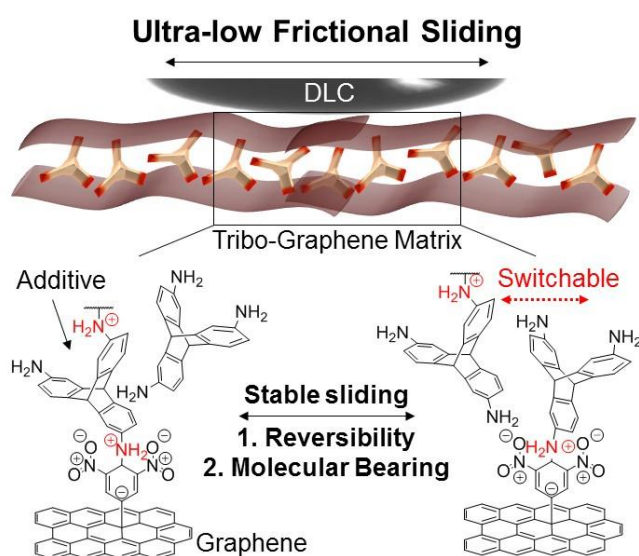
Fluid-like graphene shows macroscopic lubricity reaching a coefficient of friction of 0.01.

The rigid 3D molecular interlocking groups (Molecular bearing: triaminotriptycene, additive) create nanostructures by bonding (Stabilizer: Meisenheimer complexation) to the 3,5-dinitrophenyl functionalized graphene. Mechanical shearing converts these graphene composites into highly stable surface bound tribo-layers with a coefficient of friction (COF) ~ 0.01.

Keyword: fluid-like graphene, ultra-low friction, molecular bearing, coefficient of friction of 0.01, triptycene

Intak Jeon^{1,2†}, Geehoon Park^{3†}, Pan Wang^{1,2}, Ju Li^{4,5*}, Ian W. Hunter^{3*}, and Timothy M. Swager^{1,2*}

Dynamic Fluid-like Graphene with Ultra-Low Frictional Molecular Bearing



Supporting Information

Dynamic Fluid-like Graphene with Ultra-Low Frictional Molecular Bearing

Intak Jeon^{1,2†}, Geehoon Park^{3†}, Pan Wang^{1,2}, Ju Li^{4,5*}, Ian W. Hunter^{3*}, and Timothy M. Swager^{1,2*}

Dr. I. Jeon, Dr. P. Wang, Prof. T. M. Swager
Department of Chemistry
Institute for Soldier Nanotechnologies
Massachusetts Institute of Technology
Cambridge, MA 02139, USA
E-mail: tswager@mit.edu

G. Park, Prof. I. W. Hunter
Department of Mechanical Engineering
Massachusetts Institute of Technology
Cambridge, MA 02139, USA
E-mail: ihunter@mit.edu

Prof. J. Li
Department of Nuclear Science and Engineering
Department of Materials Science and Engineering
Massachusetts Institute of Technology
Cambridge, MA 02139, USA
E-mail: liju@mit.edu

Materials and Methods

Synthesis of 3,5-dinitrophenyl functionalized graphene (FG): Highly oriented pyrolytic graphite (HOPG) was used as the cathode in a three-electrodes electrochemical cell, containing 1.5 M tetrabutylammonium perchlorate (TBAP), acetonitrile (MeCN, 2 mL) and dimethylformamide (DMF, 2 mL) (Ag/Ag⁺ as reference electrode and graphite as counter electrode). The application of continuous voltage ramp (−3.05 to −3.25 V as −2 μV s^{−1}) induced the intercalation of tetrabutylammonium cations (TBA⁺) into graphene interlayers, resulting in Hyper-3-stage-1 graphite intercalation compound (GIC). Graphene and functionalized graphene dispersions were obtained by the following methods: (i) The Hyperstage-1 GIC was sonicated in DMF for exfoliation and then removal of the intercalated TBA⁺s was achieved by washing with MeCN and DMF. (ii) For covalent functionalization, the Hyper-3-Stage-1 GIC was added carefully an electrochemical cell, containing 0.1 M 3,5-dinitrobenzenediazonium tetrafluoroborate, 1 M TBAP and 4 mL MeCN solution. Again, continuous voltage ramp (−1.40 to −1.80 V as −2 μV s^{−1}) was passed through the Hyper-3-Stage-1 GIC. FGs were spontaneously exfoliated from the Hyper-3-Stage-1 GIC. Then the functionalized graphene sheets were collected through vacuum filtration and thoroughly washed with MeCN and DMF.

Synthesis of Trinitrotriptycenes a and b (Figure S1): Triptycene (2.0 g, 8 mmol) and concentrated HNO₃ (80 mL) were added in a round flask. The mixture was heated to 75 °C for 24 h. After cooling down to room temperature, the solution was poured into ice water. The precipitate was filtered, washed with ice water and dried. The product was further purified by column chromatography to afford a and b as white solids (a/b = 2.9/1, 1.3 g, 42% yield). Compound a (major): ¹H NMR (600 MHz, CDCl₃): δ 8.35-8.32 (m, 3H), 8.07-8.04 (m, 3H), 7.64-7.63 (m, 3H), 5.83 (s, 1H), 5.81 (s, 1H).

Synthesis of Triaminotriptycenes (Triamino-T) c and d (Figure S1): Trinitrotriptycenes a, b (1 g, 2.5 mmol) and MeOH (40 mL) were added in a flame-dried Schlenk flask. Palladium on activated charcoal was added to the solution, bubbling with hydrogen for 10 h. The mixture was then filtered through a pad of celite. The solvent was evaporated to give Triamino-T as yellow solids (c/d = 3.0/1, 0.73 g, 95% yield). Compound c (major): ¹H NMR (600 MHz, CDCl₃): δ 7.07-7.04 (m, 3H), 6.73-6.71 (m, 3H), 6.27-6.22 (m, 3H), 5.04 (s, 1H), 5.02 (s, 1H), 3.43 (br.s, 6H).

3,5-dinitrophenyl-triaminotriptycene functionalized graphene (FG-T): Figure S1 illustrates the synthesis of the functionalized graphene with 3,5-dinitrophenyl groups anchoring triaminotriptycene groups. Meisenheimer complexes form by the addition of Triamino-T to the FG (50 mg : 4 mg weight ratio) in DMF. And then FG-T was collected through a polytetrafluoroethylene (PTFE) filter membrane with 0.1 μm pore size by vacuum filtration. FG-T+: 4 mg of Triamino-T was added to the above FG-T. For a stable sliding condition, the optimal weight ratio of FG/T is from 0.017 to 1.

Rheometric measurements of graphenes: Graphene dispersions were deposited on a substrate and cut them to the appropriate size for rheometric tests. Graphenes were measured on a TA AR2000 rheometer in a 25-mm-diameter plate-plate geometry at 25 °C. Frequency sweeps were performed by applying a sinusoidal strain, $\gamma = \gamma_0 \sin(\omega t)$, with $\gamma_0 = 0.5\%$, within the linear viscoelastic range.

Graphene assembly: Graphene solutions were dispersed into DMF with the aid of sonication to generate a uniform and stable graphene solution. The FG and FG-T+ solutions were

1 dispersed in DMF. These graphenes assembled into uniform films on the surface of water
2 when several drops of ethyl acetate were added to the dispersion in dimethylformamide
3 (DMF) that had been added to water (**Figure S1**). In this process the graphene moves to the
4 water-air surface by Rayleigh-Bénard convection and then simultaneously assemble into an
5 interconnected films driven by Marangoni forces. The film is then transferred onto a stainless
6 steel (SS) substrate (**Figure S1**). After transfer, solvent is removed by vacuum evaporation at
7 room temperature for 30 min. The SS plate samples were cleaned by sonication in acetone
8 and isopropanol alcohol to remove any organic contaminants and then kept in a dry chamber.
9 This densely covered surface was required to prevent the DLC from directly contacting the SS
10 (grade 316) substrate.
11

12
13 *Friction characterization:* The friction measurement system, shown in **Figure S4**, consists of
14 a linear flexure bearing stage driven linearly back and forth by a custom built Lorenz force
15 motor, two load cells connected in series and perpendicularly to each other, a stepper motor
16 driving the sensor assembly up and down, and an environmental chamber in which the
17 measurement system is enclosed. A reconfigurable input-output (cRIO) system (cRIO-9024,
18 National Instruments) was used to control the velocity of the bearing stage and the normal
19 force applied on the sample. To quantify COF ($\mu = F_f/F_n$) the DLC ball slides back and forth
20 (linear velocity: 16 to 52 mm s⁻¹) repeatedly along a horizontal line on a film, while
21 simultaneously measuring frictional force (F_f) and normal force (F_n). The resolutions of each
22 load cell are 5 mN (normal) and 0.5 mN (lateral), and forces are sampled at 1 kHz. 3 N of
23 normal force was applied to the SS plate by moving the DLC-coated (a-C:H, Richter precision
24 inc.) SS ball (grade 440C, diameter of 9.5 mm), attached at the tip of the sensor assembly,
25 down to the sample on the moving bearing stage. The sample on the bearing stage slides 4
26 mm backward and forward against the DLC-coated SS ball and the linear velocity was
27 maintained constant as 16 mm s⁻¹ during the measurement. All measurements were conducted
28 at room temperature. The COF was calculated by dividing the measured frictional force by
29 normal force and averaged over each backward and forward cycle to generate one data point
30 on the COF plot. The first and the last 5 % of the measured COFs in each cycle were omitted
31 as they reflect the static friction of the materials. Friction experiments were repeated more
32 than three times for each sample in order to ensure the reliability. After the friction test, the
33 tribo-layer on the wear track were collected to investigate the structure of films. To validate
34 the accuracy of our custom built friction measurement setup, the friction coefficient of
35 stainless steel ball (grade 440C, diameter of 9.5 mm) against a Teflon sheet (thickness of 0.9
36 mm) is measured and compared to data presented in other literature^[1,2] (see **Figure S5**). The
37 sliding speed of the experiments is 2.5 mm s⁻¹ and normal force of 1.5 N, 3 N and 6 N are
38 used to vary the normal pressure of the contact. The contact areas are approximated based on
39 the optical and SEM images of the Teflon sheet after the experiments. As is shown, the
40 measured COFs are ranging in between 0.018 and 0.026, comparable to the data reported by
41 Thompson et al.^[1] and Mokha et al.^[2]. However, in our result, the trend of lower COFs with
42 higher normal pressures are not observed. This can be attributed to the difference in
43 calculating the normal pressure of the contact: the contact area is assumed to be held constant
44 with different normal forces in the literature whereas it is observed to change as the Teflon
45 sheet at the contact deforms.
46
47
48
49
50
51
52
53

54 *Nanoindentation:* Instrumented nanoindentation experiments were performed using a
55 Triboindenter (Hysitron 950) at room temperature, calibrated on fused quartz. The FG-T+
56 tribo-layer was used after sliding test. During indentation process, the displacements versus
57 the applied loads are recorded. Those records are then used to calculate the indentation
58 hardness of the FG-T+ tribo-layer. Each point is separated by a distance of 2 μm .
59
60
61
62
63
64
65

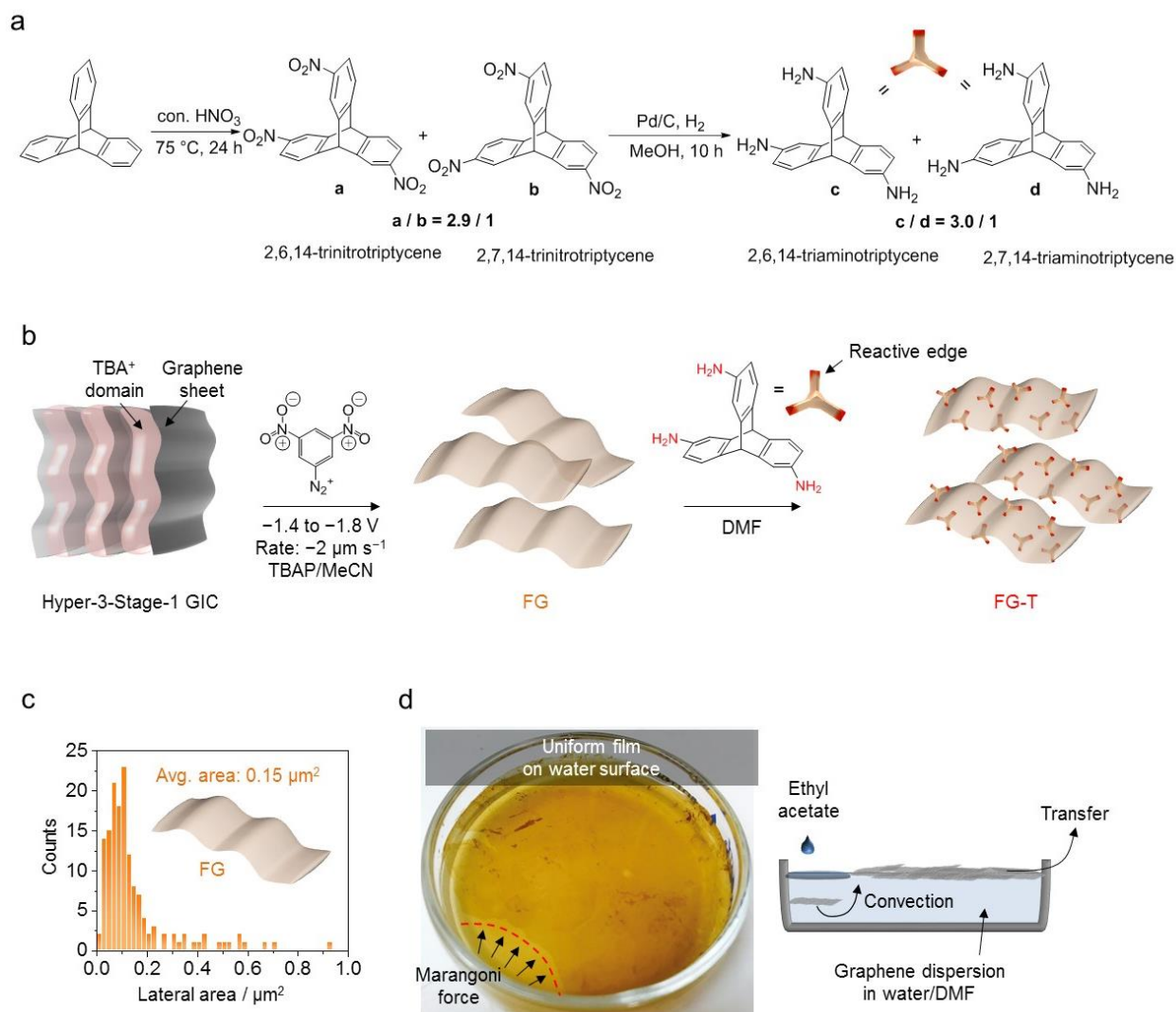


Figure S1. (a) Synthesis of Triamnio-T. (b) FG-T from Hyper-3-Stage-1 graphite intercalation compound (GIC). The Hyper-3-Stage-1 GIC represents the expanded gallery with intercalated tetrabutylammonium ion (TBA^+) domains between the basal planes of graphenes (TBAP = tetrabutylammonium perchlorate). (c) The size distribution of FG. (d) The optical micrograph of a graphene film on water surface. The graphene assembly on water surface is driven by Rayleigh–Bénard convection and Marangoni force.

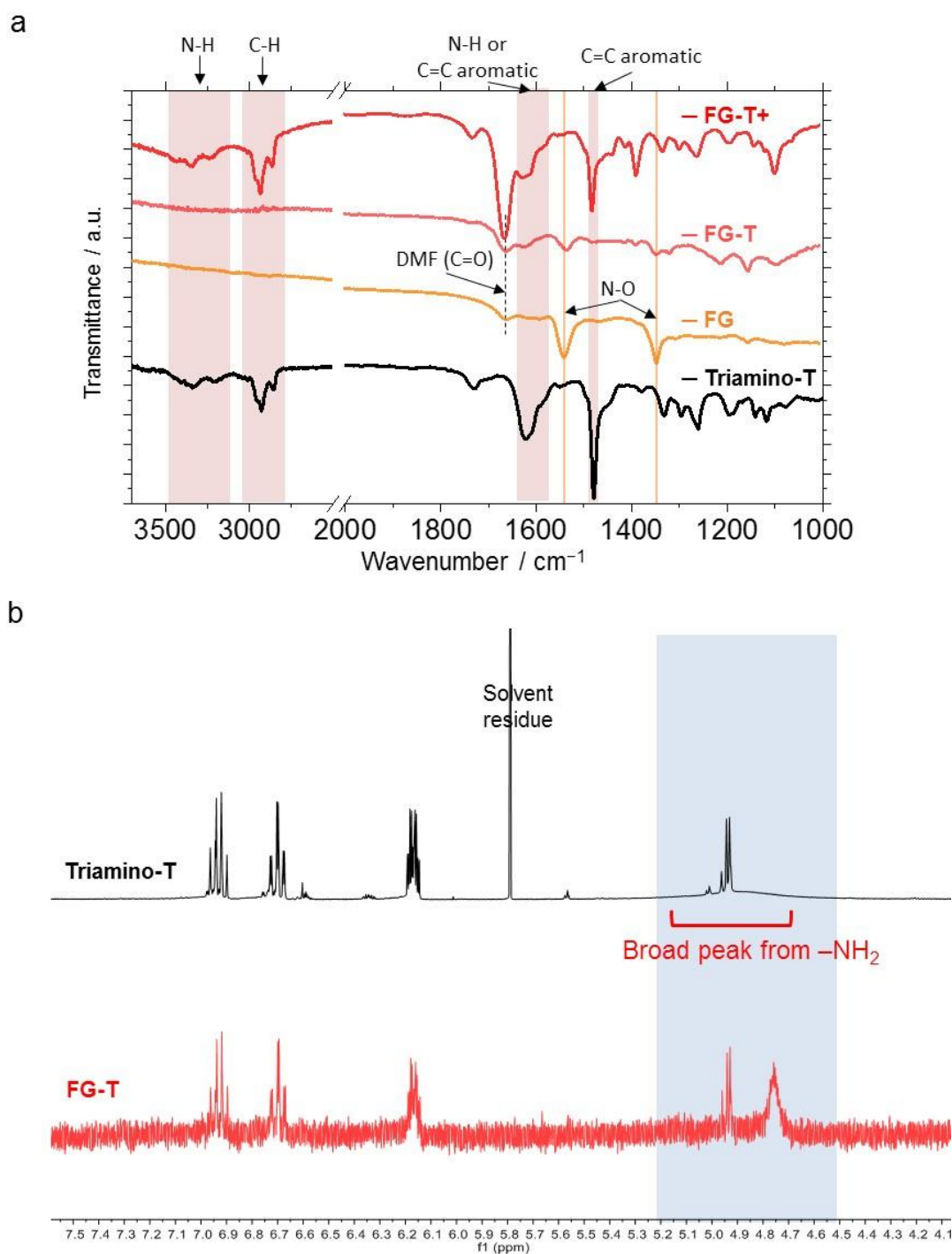


Figure S2. (a) Attenuated total reflectance Fourier transform infrared spectroscopy (ATR-FTIR) data of Triamino-T, FG, FG-T, and FG-T+. (b) Nuclear magnetic resonance spectroscopy (NMR) spectra of FG-T, and Triamino-T. FG-T (major): ^1H NMR (400 MHz, DMF- d_7): δ 6.96-6.90 (m, 3H), 6.72-6.67 (m, 3H), 6.19-6.14 (m, 3H), 4.91 (s, 1H), 4.93 (s, 1H), 4.76 (br.s, 6H).

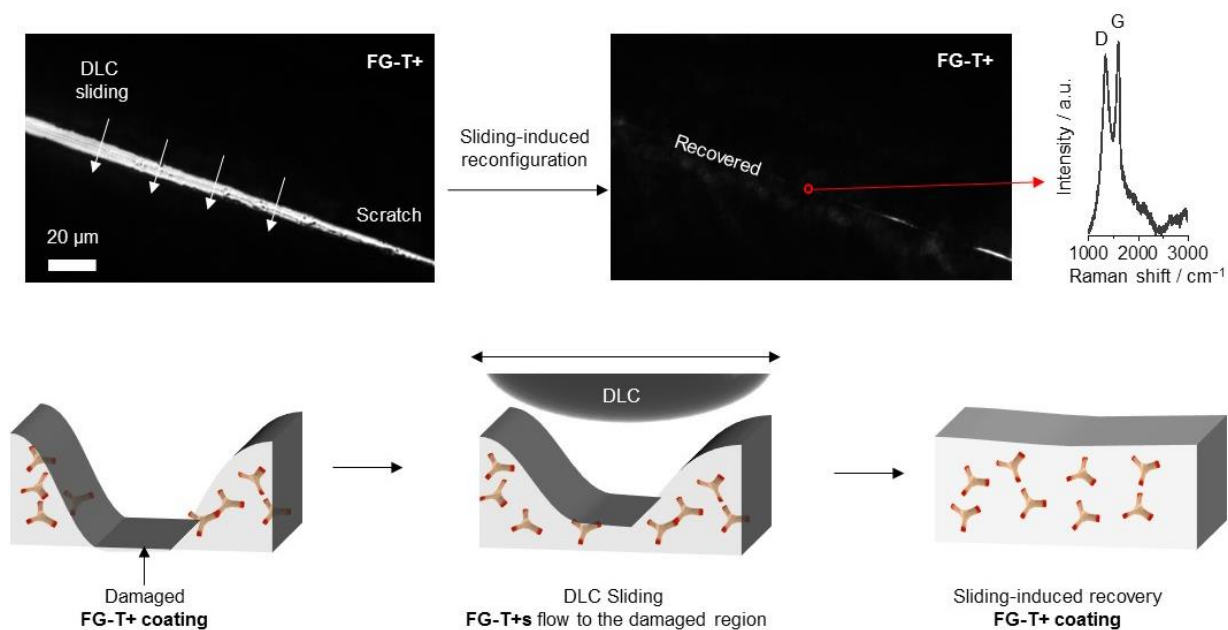
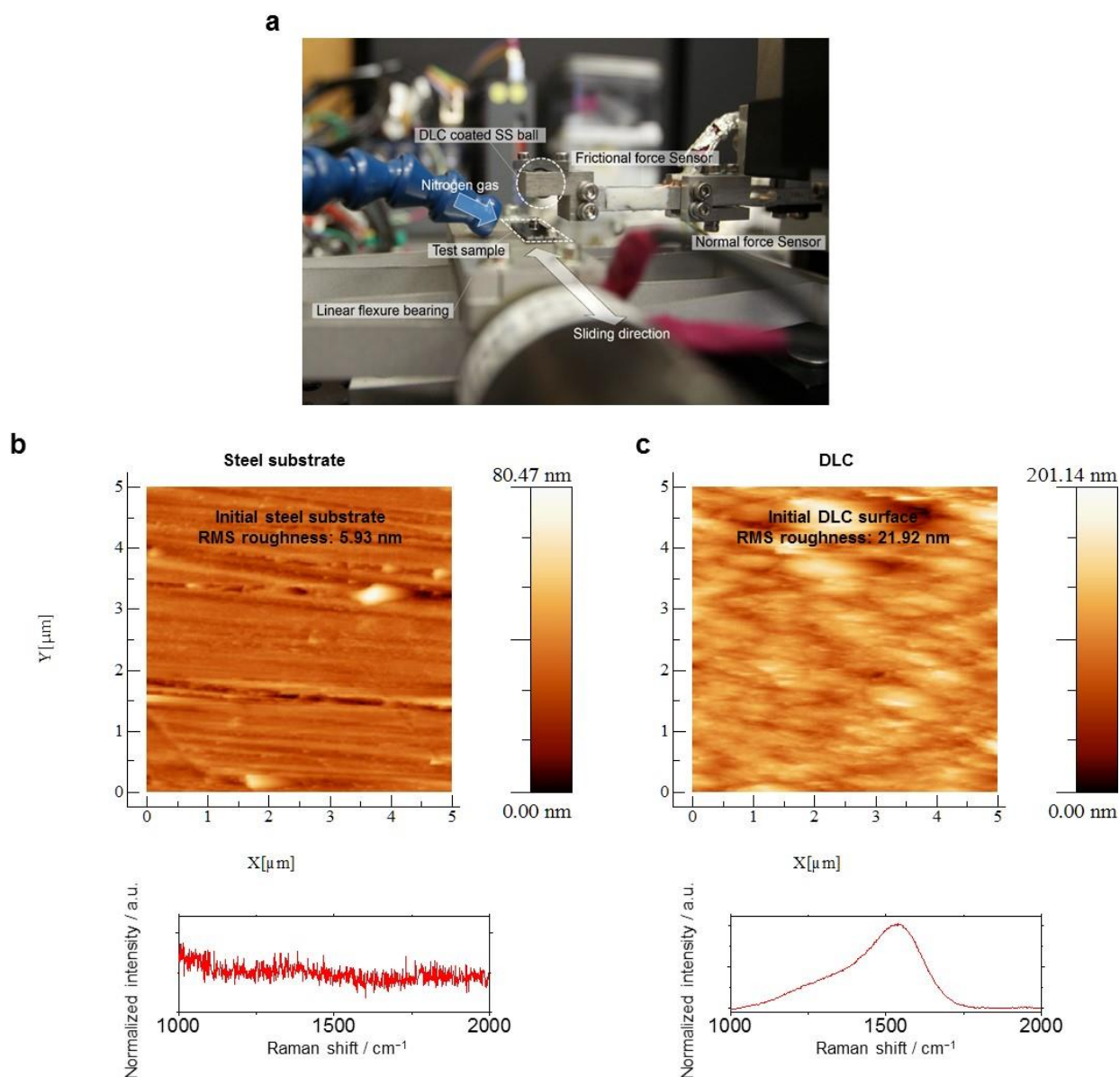


Figure S3. Top: Mechanical sliding-induced reconfiguration of a scratched FG-T+ film: The reversible Meisenheimer complexes across the cracked film (intentionally scratched by a razor blade) was cured under mechanical shear force. Raman signature of FG-T+ from the recovered region. Bottom: Schematic illustration showing the formation of a tribo-layer against a DLC-coated SS ball.



41 **Figure S4.** (a) Experimental demonstration and coefficient of friction (COF) results of
42 graphene films. An image of the linear tribometer equipped with a DLC-coated SS ball. Tests
43 were performed at room temperature (RT) under 3 N load (contact pressure: 0.3 ~ 0.4 GPa).
44 Each sample was tested more than three times in order to ensure the reliability. The tapping-
45 mode atomic force microscopy (AFM) surface scans and the Raman spectra of (b) a SS
46 substrate, and (c) a DLC-coated SS ball.
47
48
49
50
51
52
53
54
55
56
57
58
59
60
61
62
63
64
65

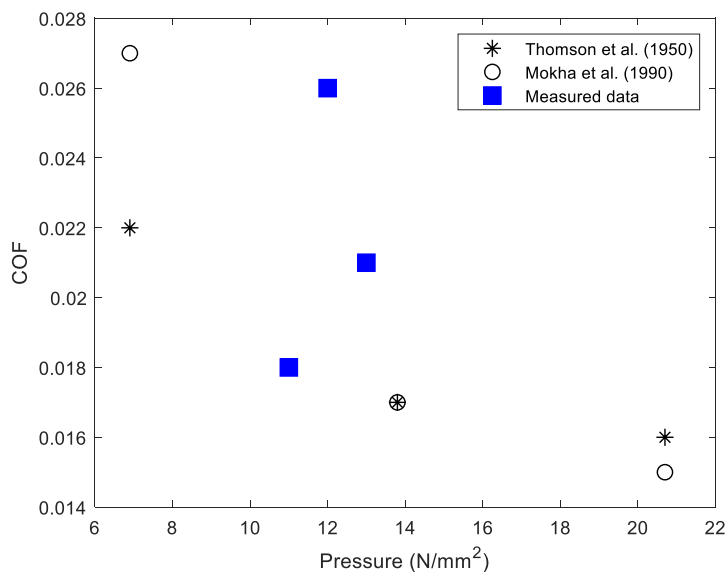


Figure S5. Comparison of the COF between stainless steel balls and Teflon sheets measured by the custom-built linear macro tribometer and the data from literature.^[1,2] The ball diameter of 9.5 mm is used to slide at the linear speed of 2.5 mm s⁻¹ on the Teflon sheet of 0.9 mm thickness. The contact pressures for the normal force of 1.5 N, 3 N and 6 N are estimated to be 12 N mm⁻², 13 N mm⁻², and 11 N mm⁻², respectively.

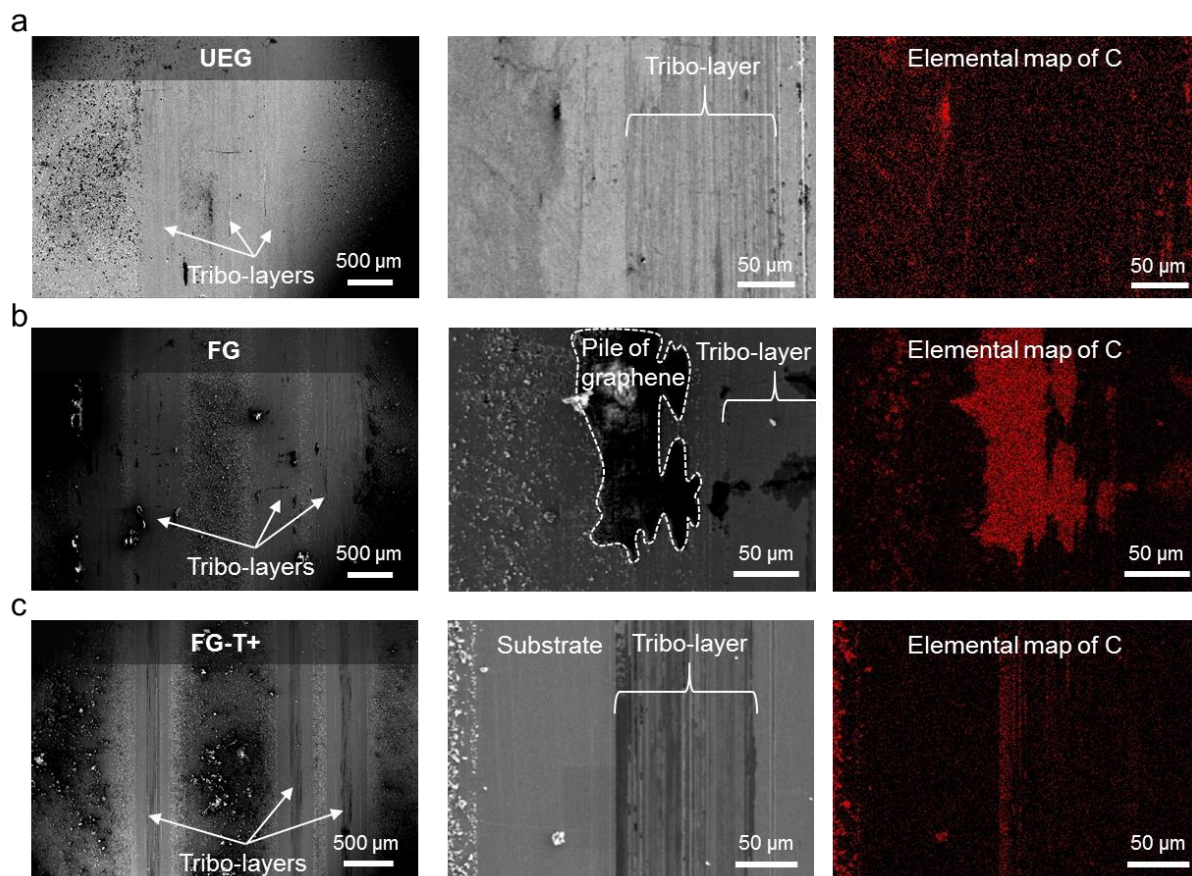


Figure S6. (a) Scanning electron microscope (SEM) images with the corresponding energy dispersive X-ray spectroscopy (EDS) carbon mapping of UEG, (b) FG, and (c) FG-T+ after sliding.

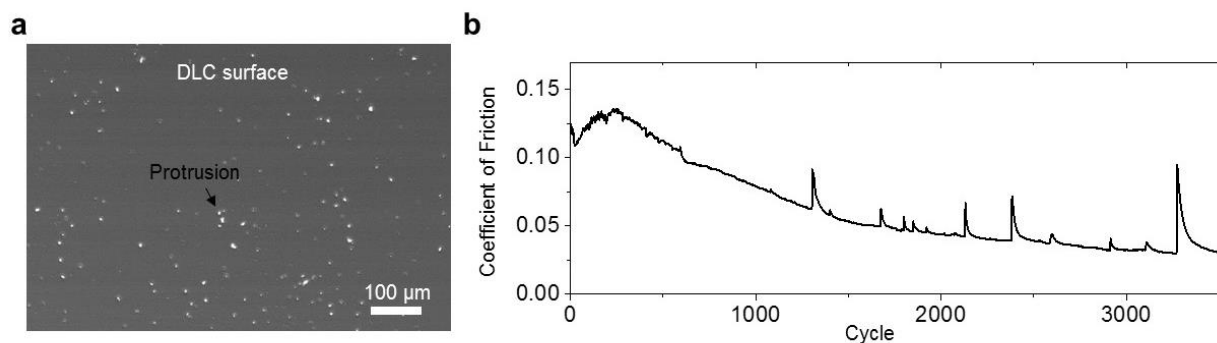


Figure S7. (a) A SEM image of the surface of diamond-like-carbon (DLC)-coated ball. The sliding motions with the rough surface at contact edges highly cause the damages of coated materials. (b) The COF for DLC-coated ball sliding against UEG. As a result of the unstable tribo-layer formation on the SS substrate, the COF increases at the beginning of sliding and many large COF spikes appear. Similarly, graphene films on SiO₂ surfaces display a substantial amount of variance in the COF in sliding experiments against a DLC ball.^[3] This erratic nature of COF of pristine graphene coatings at macroscale levels will limit the operational lifespan of a mechanical components and/or require frequent reapplication of the lubricant.

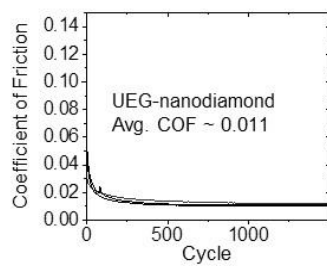


Figure S8. The COF of UEG-nanodiamond in our system. The average of COF is 0.011.

1
2
3
4
5
6
7
8
9
10
11
12
13
14
15
16
17
18
19
20
21
22
23
24
25
26
27
28
29
30
31
32
33
34
35
36
37
38
39
40
41
42
43
44
45
46
47
48
49
50
51
52
53
54
55
56
57
58
59
60
61
62
63
64
65

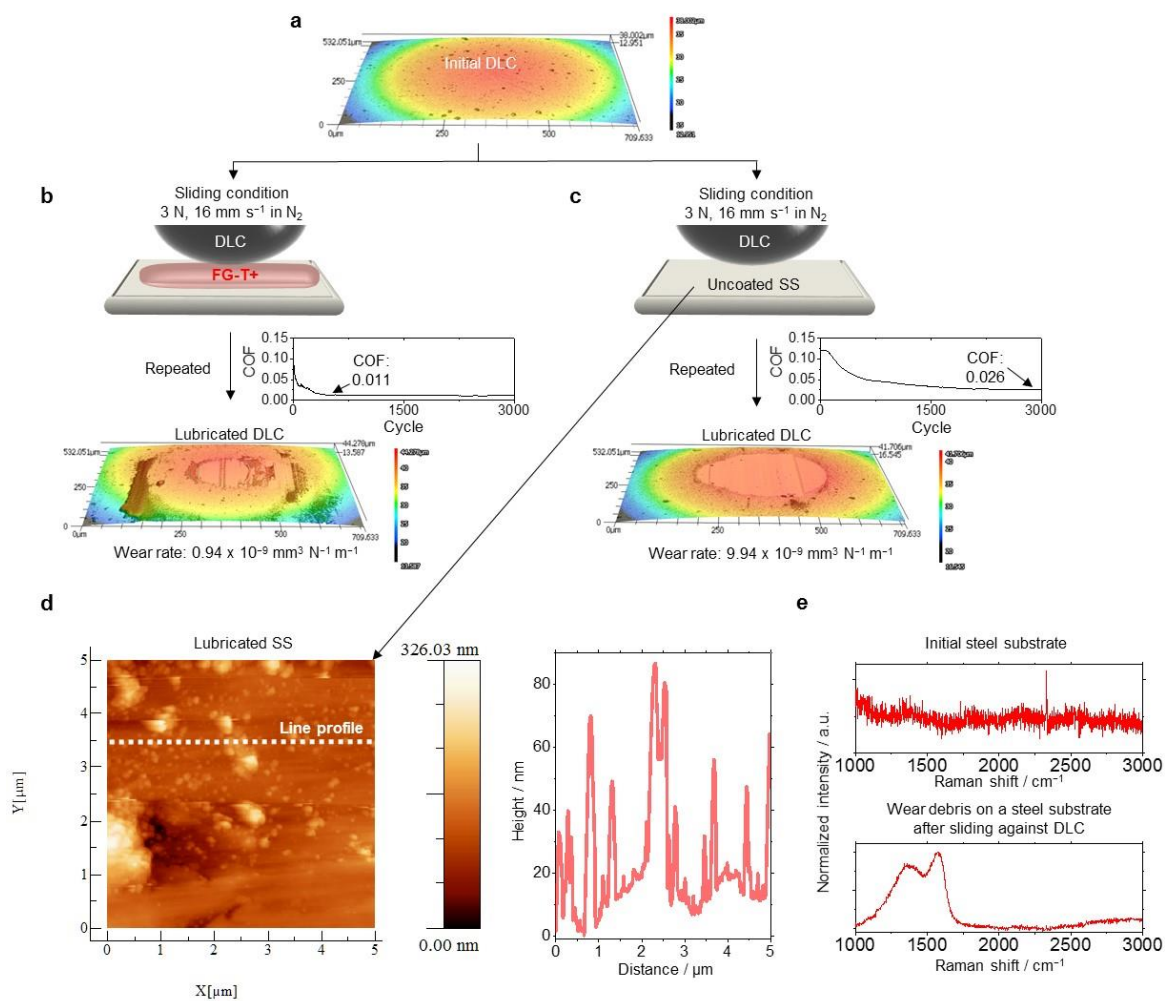


Figure S10. (a) The optical profile of a DLC-coated SS ball before a friction test. The optical profile and the COF of an intact DLC-coated SS ball against (b) a **FG-T+**-coated SS substrate and (c) an uncoated SS substrate in N_2 environment. (b) Over 20000 cycles, the wear rate of DLC-coated SS ball against **FG-T+** on a SS substrate is $0.94 \times 10^{-9} \text{ mm}^3 \text{ N}^{-1} \text{ m}^{-1}$. (c) The wear rate of DLC-coated SS ball against an uncoated SS substrate is $9.94 \times 10^{-9} \text{ mm}^3 \text{ N}^{-1} \text{ m}^{-1}$. (d) An AFM surface scan of the uncoated SS substrate after sliding against a DLC-coated SS ball. We observed that the tribo-chemically generated particles due to the wear of a DLC/SS pair. The morphology is different from the **FG-T+** in **Figure 4d** in main text. (e) Raman spectra of a SS substrate before and after sliding against DLC.

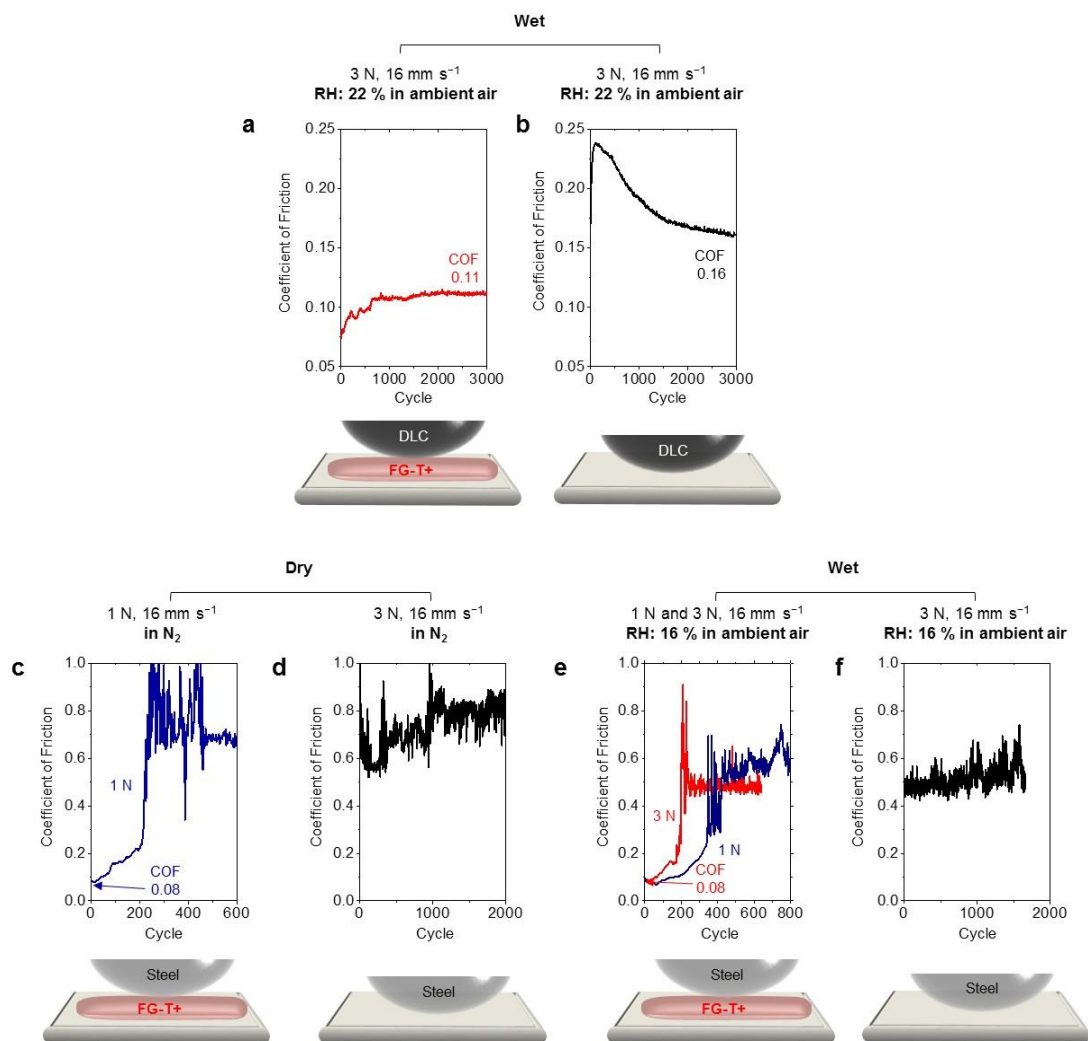


Figure S11. The COF of a DLC-coated ball against (a) a FG-T+-coated SS substrate, and (b) a SS substrate in ambient environment. The COF of an uncoated SS ball against (c) a FG-T+-coated SS substrate and (f) a SS substrate in N₂ environment. The COF of an uncoated SS ball against (e) a FG-T+-coated SS substrate, and (f) a SS substrate in ambient environment.

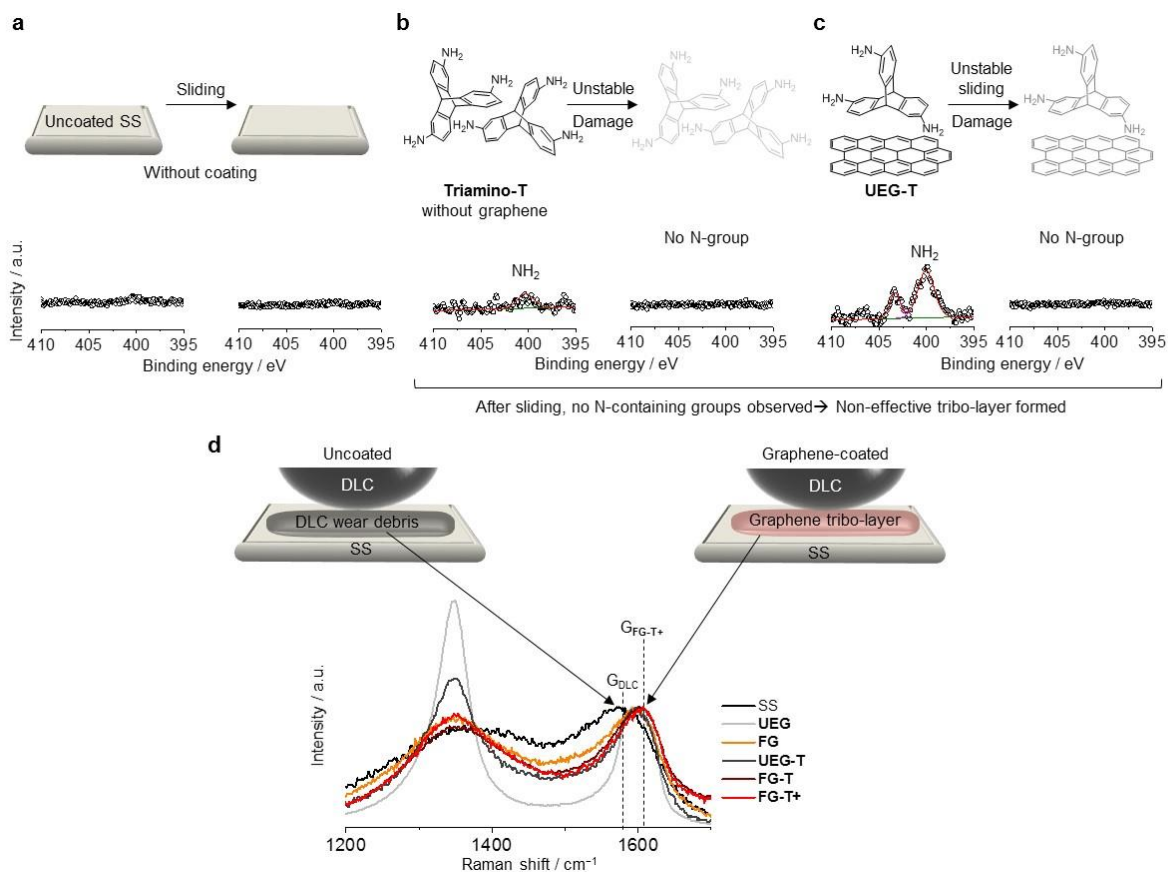


Figure S12. XPS spectra of (a) uncoated SS, (b) Triamino-T, and (c) UEG-T before/after sliding against DLC. During sliding, the Triamino-T and UEG-T also undergo tribo-chemically damage that causes unstable frictional sliding. (d) Raman spectra of the tribo-layer of uncoated SS, UEG, FG, UEG-T, UEG-T, FG-T, and FG-T+ after sliding against DLC. The tribo-layers of graphenes clearly show different chemical signatures after sliding against DLC, compared with the tribo-layer of uncoated SS. For example, the G_{FG-T+} band (1606 cm^{-1}) of the tribo-layer of FG-T+ is distinguishable from the G_{DLC} -band (1578 cm^{-1}) of DLC debris.

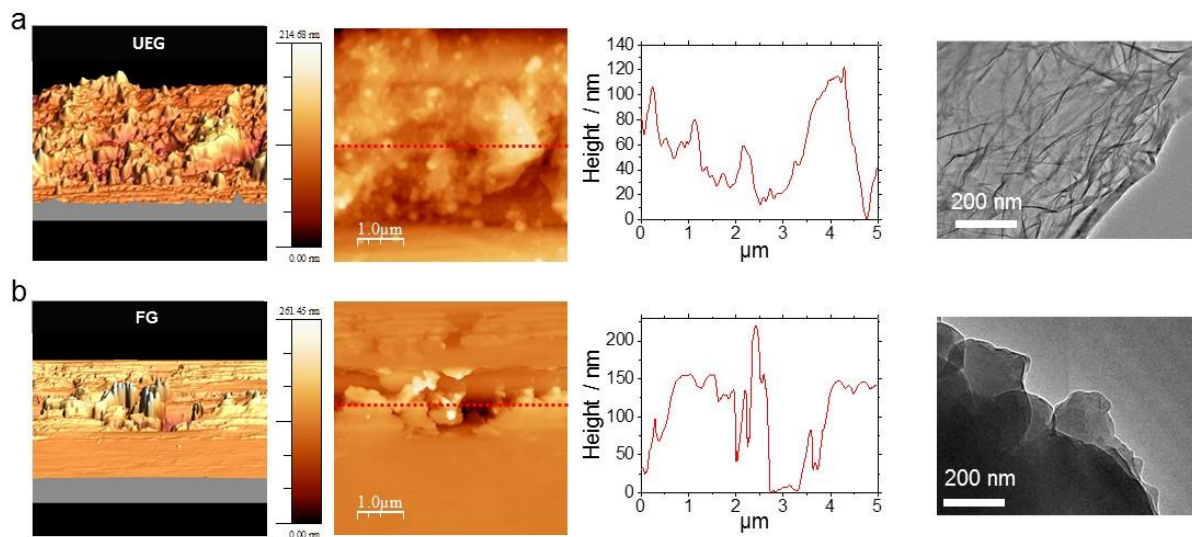


Figure S13. AFM surface scans and TEM data of (a) UEG, and (b) FG tribo-layers.

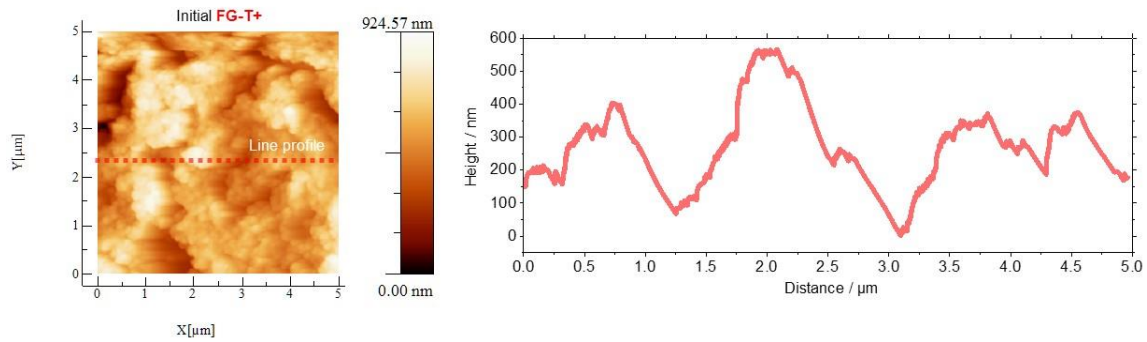


Figure S14. AFM surface scan of the initial FG-T+ coating on a SS substrate before a friction test.

Reference

- [1] J. B. Thompson, G. C. Turrell, B. W. Sandt, *SPE Journal* **1995**, 11, 13
- [2] A. Mokha, M. Constantinou, A. Reinhorn, *Journal of Structural Engineering* **1990**, 116, 438.
- [3] D. Berman, S. A. Deshmukh, S. K. R. S. Sankaranarayanan, A. Erdemir, A. V. Sumant, *Science* **2015**, 348, 1118



Click here to access/download
Production Data
Figure1.tif



Click here to access/download
Production Data
Figure2.tif



Click here to access/download
Production Data
Figure3.tif



Click here to access/download
Production Data
Figure4.tif